Cell Reports
Article

Functional Activation of ATM by the Prostate Cancer Suppressor NKX3.1

Cai Bowen,[1,2] Jeong-Ho Ju,[1,2] Ji-Hoon Lee,[3,4,5] Tanya T. Paull,[3,4,5] and Edward P. Gelmann[1,2,*]
[1]Department of Medicine, Herbert Irving Comprehensive Cancer Center, Columbia University, 177 Fort Washington Avenue, MHB 6N-435, New York, NY 10032, USA
[2]Department of Pathology, Herbert Irving Comprehensive Cancer Center, Columbia University, 177 Fort Washington Avenue, MHB 6N-435, New York, NY 10032, USA
[3]The Howard Hughes Medical Institute, University of Texas at Austin, Austin, TX 78712, USA
[4]Department of Molecular Genetics and Microbiology, University of Texas at Austin, Austin, TX 78712, USA
[5]Institute for Cellular and Molecular Biology, University of Texas at Austin, Austin, TX 78712, USA
*Correspondence: gelmanne@columbia.edu
http://dx.doi.org/10.1016/j.celrep.2013.06.039

SUMMARY

The prostate tumor suppressor NKX3.1 augments response to DNA damage and enhances survival after DNA damage. Within minutes of DNA damage, NKX3.1 undergoes phosphorylation at tyrosine 222, which is required for a functional interaction with ataxia telangiectasia mutated (ATM) kinase. NKX3.1 binds to the N-terminal region of ATM, accelerates ATM activation, and hastens the formation of γhistone2AX. NKX3.1 enhances DNA-dependent ATM kinase activation by both the MRN complex and H_2O_2 in a DNA-damage-independent manner. ATM, bound to the NKX3.1 homeodomain, phosphorylates NKX3.1, leading to ubiquitination and degradation. Thus, NKX3.1 and ATM have a functional interaction leading to ATM activation and then NKX3.1 degradation in a tightly regulated DNA damage response specific to prostate epithelial cells. These findings demonstrate a mechanism for the tumor-suppressor properties of NKX3.1, demonstrate how NKX3.1 may enhance DNA integrity in prostate stem cells and may help to explain how cells differ in their sensitivity to DNA damage.

INTRODUCTION

To combat threats imposed by DNA damage, cells have evolved the DNA damage response to detect newly created genetic lesions, signal their presence, and initiate repair (Ciccia and Elledge, 2010; Jackson and Bartek, 2009). Cells that are defective in these mechanisms display heightened sensitivity to DNA-damaging agents and in some instances are prone to cancer. It is widely appreciated that the prostatic epithelium is subject to DNA damage due to inflammation in the aging prostate gland (Nelson et al., 2003; Shen and Abate-Shen, 2010). We have shown that the prostate gatekeeper suppressor NKX3.1 plays a significant role in protecting against DNA damage and promoting DNA repair in the prostate, while its loss of expression predisposes the prostatic epithelium to DNA damage (Bowen and Gelmann, 2010).

NKX3.1 is a haploinsufficient prostate cancer suppressor protein that has reduced expression in the majority of human primary prostate cancers (Asatiani et al., 2005). NKX3.1 downregulation also likely predisposes to the formation of invasive prostate cancer, since decreased expression is seen in premalignant lesions and prostatic intraepithelial neoplasia (PIN) (Asatiani et al., 2005; Bethel et al., 2006). During prostate cancer progression, there is progressive loss of NKX3.1 expression, suggesting that there is selective pressure against expression of this suppressor protein (Bowen et al., 2000). NKX3.1 downregulation results from genetic loss, DNA methylation, or both, and in addition, NKX3.1 turnover is accelerated by ubiquitination and proteasomal degradation triggered by cellular exposure to inflammatory cytokines (Asatiani et al., 2005; Markowski et al., 2008). In this way, regions of inflammatory atrophy may cause both downregulation of NKX3.1 and oxidative damage that accompanies inflammation (Bethel et al., 2006). Inflammation is known to predispose surrounding cells to oxidative damage and, as a result, cause procarcinogenic mutations (Murata et al., 2012). In fact, in regions of bacterial prostatitis, another inflammatory risk factor for prostate cancer, NKX3.1 expression was also seen to be decreased (Khalili et al., 2010).

The DNA damage response may be activated directly by agents that can induce DNA damage or by the presence of intracellular free oxygen radicals (Ciccia and Elledge, 2010; Jackson and Bartek, 2009). An early step in the DNA damage response is the rapid accumulation of damage-signaling proteins at the damage site, corresponding to the sensor complex of the proteins MRE11, Rad50, and NBS1 (MRN complex) (Bekker-Jensen et al., 2006). This is followed by recruitment of the transducer proteins MDC1 and 53BP1. Interestingly, 53BP1 is both an interacting protein of and substrate for ataxia telangiectasia mutated (ATM), and is used experimentally as an index of ATM activation. ATM is one of three DNA-dependent PI3 kinase-like proteins (the others being DNA-dependent protein kinase [DNA-PK] and

ataxia telangiectasia and Rad3-related [ATR]) that mediate the early response to DNA damage (for review, see Kurz and Lees-Miller, 2004). ATM phosphorylates the histone variant H2AX and downstream effectors, including the Chk1 and Chk2 cell-cycle kinases (Bartek and Lukas, 2003; Lee and Paull, 2004, 2005; Paull and Lee, 2005). Thus, ATM serves as a key transducer of DNA damage signals in mammalian cells being activated in part by the MRN complex bound to double-stranded breaks to signal through phosphorylation of H2AX and a myriad of other substrates (Fernandez-Capetillo et al., 2004; Kurz and Lees-Miller, 2004). Furthermore, ATM also reacts to levels of reactive oxygen species and may act as a cellular sensor for oxidative potential (Ditch and Paull, 2011).

Upon activation by DNA damage, ATM undergoes autophosphorylation at serine 1981 (S1981) and three other (S/T)Q sites favored for ATM substrates (for review, see Ditch and Paull, 2011). ATM also is activated by oxidative stress independently of DNA damage (Guo et al., 2010b). Since oxidative stress may be a major source of DNA damage in the prostate, ATM may play a major role in protecting prostate epithelial cells from DNA damage induced by oxidative stress. ATM undergoes extensive phosphorylation after DNA damage, including phosphorylation at S1981 that is used as an experimental marker for ATM activation. However, missense mutation of several of the ATM phosphorylation sites in mice, including the site analogous to S1981, demonstrated that they were not essential for at least some aspects of ATM activation (Daniel et al., 2008).

We have previously shown that NKX3.1 enhances cell survival after DNA damage and that NKX3.1 enhances the DNA damage response by increasing ATM activation and γH2AX accumulation at the damage site (Bowen and Gelmann, 2010). We now demonstrate that the importance of NKX3.1 to the stem cell may be via enhancement of the DNA damage response mediated by ATM.

RESULTS

NKX3.1 Affects the ATM Response to DNA Damage

NKX3.1 colocalizes with γH2AX to sites of DNA damage induced by laser microirradiation (LMI) (Bowen and Gelmann, 2010). Moreover, NKX3.1 can be found bound at a site of double-strand DNA breakage, as shown by chromatin immunoprecipitation (ChIP) of NKX3.1 at a DNA cleavage site introduced into 293T cells and cut by the I-SceI restriction endonuclease (Figure 1A). Changing the expression level of NKX3.1 either by small interfering RNA (siRNA) knockdown in LNCaP cells or by exogenous expression of NKX3.1 in PC-3 cells affected the cells' acute responses to DNA damage. Within 5 min of DNA damage induced by LMI, the accumulation of ATM, phosphorylated ATM at S1981 (pATM(S1981)), and γH2AX at DNA damage sites was affected by changes in NKX3.1 expression levels (Figure 1B). Quantitation of γH2AX and pATM(S1981) at the DNA damage site at 1 min intervals showed that NKX3.1 expression affected both the rate and the magnitude of protein accumulation (Figure S1A). We confirmed the effects of NKX3.1 knockdown in the LNCaP(si471) cells by using si3098, another NKX3.1 silencing construct that we previously described (Bowen and Gelmann, 2010), to ensure that the effect on NKX3.1 downregulation was not unique to a single siRNA, thus decreasing the likelihood of off-target effects (Figure S1B). In contrast to the response of ATM, we saw little effect of NKX3.1 expression on the intracellular localization of ATR (Figure 1B, bottom panels). Whereas ATM localization to the laser wound was enhanced >3-fold by the expression of NKX3.1 in PC-3 cells, ATR localization was increased by <2-fold. We previously demonstrated that enhanced phosphorylation of the ATR substrate CHK1 occurred in the presence of NKX3.1, but the ATR activation followed ATM phosphorylation chronologically (Bowen and Gelmann, 2010). The effect of NKX3.1 expression on γH2AX localization at DNA damage sites was mediated at least in part by ATM, since the ATM inhibitors Ku55933 and caffeine both diminish the effect of NKX3.1 on H2AX phosphorylation, thus implicating an interaction between NKX3.1 and ATM as a mechanism whereby NKX3.1 affects the DNA damage response (Figure 1C). A very similar response was seen when LNCaP(siLuc) and LNCaP(si471) cells were exposed to 10Gy γ-irradiation (Figure 1D). Furthermore, ATM phosphorylation was also demonstrated in situ after γ-irradiation of LNCaP cells (Figure S1C). Moreover, knockdown of NKX3.1 in LNCaP cells was shown using two different interfering RNA sequences, thus decreasing the likelihood of off-target effects by the siRNAs in this experimental system. The opposite effect on the DNA repair response was seen in PC-3 cells engineered to express NKX3.1 (Figure 1C).

To determine whether NKX3.1 directly affected ATM activity, we performed an in vitro assay using affinity-purified, epitope-tagged ATM that was incubated with purified P53 and NKX3.1. In vitro phosphorylation of P53 at serine 15 (S15), a known target site for ATM kinase (Khanna et al., 1998), was enhanced in correlation with the amount of NKX3.1 added to the reaction that included tagged ATM (Figure 2A). However, there was no effect of NKX3.1 on pP53(S15) when the experiment was reproduced with a kinase-inactivated ATM expression construct (Figure 2B). Addition of NKX3.1 to an in vitro kinase reaction also decreased the concentration threshold at which ATM activity was seen (Figure 2C). As predicted by the in vitro reconstitution experiments, P53 phosphorylation was reduced by NKX3.1 knockdown in LNCaP cells subjected to irradiation and probed for Flag-tagged ATM, and also in heterologous 293T cells expressing both Flag-ATM and MYC-NKX3.1 (Figure 2D). NKX3.1 also activated ATM kinase in vitro in an ATM activation reaction reconstituted with purified reaction components (Lee and Paull, 2005). Purified recombinant NKX3.1 enhanced the activation of ATM by the MRN complex and DNA (Figure 2E). Interestingly, mutations of the homeodomain that inhibited binding of NKX3.1 to its cognate DNA binding domain, T179A (Gelmann et al., 2002) and N174Q (Bowen and Gelmann, 2010), did not interfere with the protein-protein interaction between NKX3.1 and ATM even though these mutations had attenuated the effect of NKX3.1 on ATM in whole cells (Bowen and Gelmann, 2010). Activation of ATM by oxidation was enhanced substantially more by NKX3.1 than was activation by the MRN complex (Guo et al., 2010a, 2010b; Figure 2F). Thus, purified NKX3.1 has a direct effect on ATM activation in vitro by both double-stranded DNA breaks and H_2O_2. In LNCaP cells exposed to H_2O_2, we observed that the presence of NKX3.1 enhanced ATM phosphorylation as compared with LNCaP cells with NKX3.1 knockdown (Figure 2G).

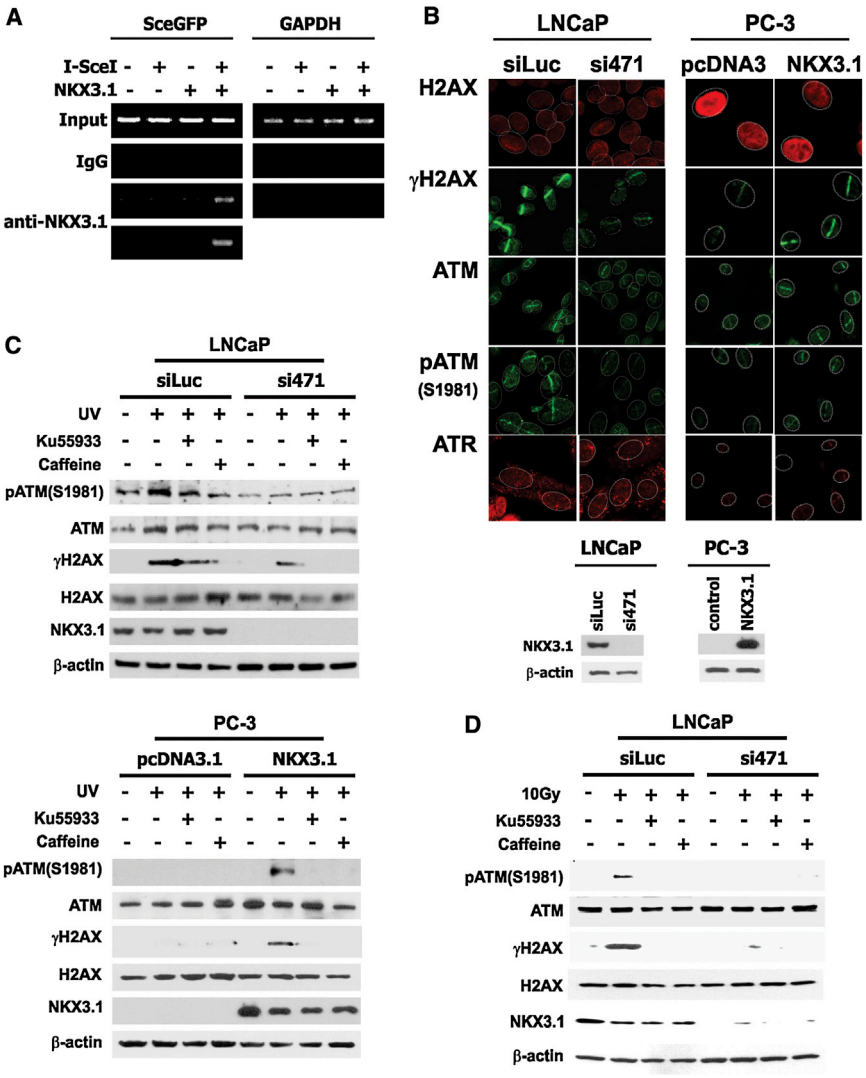

Figure 1. NKX3.1 Affects Response to DNA Damage of ATM

(A) 293T cells engineered with a single I-SceI cleavage site were transfected with an I-SceI expression vector with or without expression of NKX3.1. ChIP analysis of sequences of the GFP coding region at the cleavage site showed accumulation of NKX3.1.

(B) LNCaP cells stably transfected with control or NKX3.1 knockdown lentiviral vector (Bowen and Gelmann, 2010) or PC-3(pcDNA3) and PC-3(NKX3.1) stable cell lines were pretreated with 10 μM of BrdU overnight and 10 μg/ml of Hoechst 33258 dye for 30 min. Cells were exposed to LMI at power 36, focus 61, speed 20, and fixed 2–5 min after irradiation. Immunofluorescent detection of proteins was done as indicated on the left. An immunoblot demonstrating expression of NKX3.1 in the target cell lines is shown.

(C) LNCaP and PC-3 cells engineered for NKX3.1 knockdown or expression were treated with 10 mJ/cm^2 UV irradiation and additionally pretreated with either 10 μM Ku55933 or 2 mM caffeine for 30 min. Cells were pretreated with BrdU and Hoechst 33258 dye as above prior to UV irradiation and harvested after 10 min for immunoblotting. The presence of γH2AX in LNCaP cells treated with Ku55933 may be due to phosphorylation by ATR, DNA-dependent protein kinase, or other enzymes.

(D) LNCaP(siLuc) and LNCaP(si471) cells were pretreated as in (C) prior to irradiation with 10 Gy. Cells were harvested after 10 min for immunoblotting.

See also Figure S1.

We also asked whether NKX3.1 binding to ATM was favored by ATM phosphorylation that resulted from ATM activation. ATM is a homodimer in the inactive state and is dissociated upon activation after DNA damage by means of transphosphorylation at S1981 (Bakkenist and Kastan, 2003). ATM undergoes phosphorylation after DNA damage at a number of other residues as well. We observed increasing levels of ATM phosphorylation at S1981 during the first 20 min after DNA damage (Figure 2H, left panel). In reciprocal pull-down experiments, increasing amounts of NKX3.1 were seen to associate with ATM at 10 and 20 min after induction of DNA damage (Figure 2H). The data suggest that pATM was a preferred binding partner for NKX3.1, suggesting that NKX3.1 affected ATM after dissociation of the ATM homodimer by transphosphorylation.

ATM Binding Domain for NKX3.1

We studied the physical association between NKX3.1 and ATM using glutathione S-transferase (GST)-fusion peptides that together covered the entire length of the ATM protein. We found that peptide GST-ATM-2 spanning amino acids 250–522 interacted most strongly with NKX3.1 (Figure 3A), and that this interaction was observed with both epitope-tagged NKX3.1 and native protein expressed in LNCaP cells (Figure 3B). The ATM-2 peptide includes the nuclear localization signal (NLS) located between amino acids 385 and 388. To determine whether this region was involved in NKX3.l binding, we performed a deletion analysis on the ATM-2 fragment. In GST pull-down experiments, NKX3.1 was shown to bind to the region C-terminal to the NLS at 431–490 (Figure 3C). The 431–490 region of ATM involves a short segment of the HEAT repeat domain. To study the interaction of NKX3.1 and ATM, we engineered an ATM construct that lacked amino acids 431–490. In response to DNA damage, this construct underwent S1981 phosphorylation comparably to full-length ATM, and also displayed nuclear localization that appeared to be similar to that of the full-length protein (Figure 3D). Thus, we were able to perform experiments comparing the activities of native ATM and ATM that lacked NKX3.1 binding capability. Deletion of this 431–490 region abrogated the association of ATM with NKX3.1 and nullified the effect of NKX3.1 on ATM phosphorylation after DNA damage (Figure 3E).

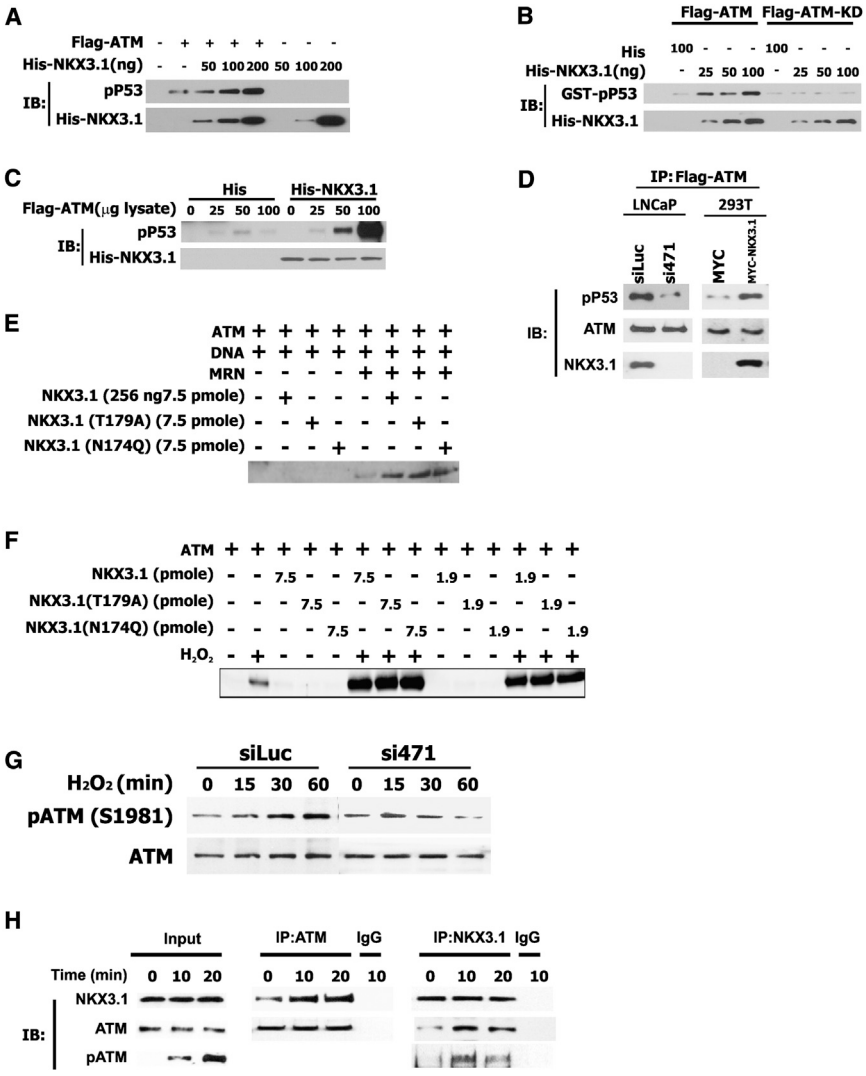

Figure 2. NKX3.1 Activates ATM In Vitro

(A) Lysates from 293T cells transfected with Flag-ATM were subjected to immunoprecipitation with 30 ml of anti-Flag M2 agarose (Sigma) for 1 hr. The Flag-ATM-bound beads were preincubated with polyhistidyl-NKX3.1 for 30 min and subsequently incubated with 1.5 mg GST-P53. P53 was resolved by SDS-PAGE and P53 phosphorylation was analyzed by immunoblotting with monoclonal antibody to phospho-P53(S15) (Cell Signaling). Levels of His-NKX3.1 were demonstrated with NKX3.1 antiserum.

(B) Lysates of 293T cells were treated as in (A) except that exogenous expression of Flag-ATM or Flag-ATM-KD was engineered.

(C) Lysates of 293T cells transfected with different amounts of Flag-ATM expression vector were exposed to anti-Flag M2 agarose, which was then washed and exposed to polyhistidine or polyhistidylNKX3.1. After a 30 min incubation, 1 mg GST-P53 was added for 60 min at 30°C. The reaction mixtures were then analyzed by immunoblotting as shown.

(D) LNCaP and 293T cells expressing the indicated vectors were subjected to immunoprecipitation and immunoblotting for pP53(S15). The uniformity of transgene expression and precipitation was confirmed by immunoblotting with monoclonal ATM antibody and NKX3.1 antiserum.

(E) Kinase assay with dimeric ATM, MRN complex, GST-P53 substrate, 10 ng linear DNA, and 256 ng NKX3.1 (wild-type [WT], T179A, and T174Q), probed with antibody directed against phosphoserine 15 of P53.

(F) Kinase assays with dimeric ATM, 0.7 mM H2O2, and 4 and 16 ng of NKX3.1 (WT, T179A, and T174Q), probed with antibody to phosphoserine15 of P53.

(G) LNCaP(siLuc) and LNCaP(si471) cells were exposed to 200 μM of H_2O_2 for the indicated times. Cell extracts were processed for immunoblotting as shown.

(H) LNCaP cells were preloaded with BrdU and pretreated with Hoechst 33528 dye prior to UV irradiation with 10 mJ/cm^2. Immunoprecipitation and immunoblotting was performed with the indicated antibodies on cell lysates from cells harvested at the indicated times.

Posttranslational Modification of NKX3.1 after DNA Damage

NKX3.1 undergoes serine and threonine phosphorylation at a number of sites that regulate protein turnover both in the steady state and in response to a number of extracellular stimuli (Li et al., 2006; Markowski et al., 2008). Because of its binding to ATM, we also asked whether NKX3.1 underwent phosphorylation on (S/T)Q sites, the preferred substrate targets for ATM kinase, thus implicating NKX3.1 as an ATM substrate. NKX3.1 p(S/T)Q was found to be increased at 30 min after irradiation and more so at 60 min after irradiation (Figure 4A). In this immunodetection experiment, we noted that the input NKX3.1 levels decreased at both 30 and 60 min after DNA damage (Figure 4A, top panel). We also observed that NKX3.1 underwent tyrosine phosphorylation within 5 min of DNA damage. (Tyrosine phosphorylation is described further below and in the data presented in Figure 6.) We previously showed that NKX3.1 turnover is regulated by phosphorylation, and therefore, because of the apparent correlation between serine/threonine phosphorylation induced by DNA damage and NKX3.1 turnover, we further examined the reduction of NKX3.1 levels suggested by the results in Figure 4A. UV exposure of LNCaP cells preloaded with bromodeoxyuridine (BrdU) and treated with Hoechst 33258 dye resulted in decreased levels of NKX3.1 within 30 min (Figure 4B). The decline in NKX3.1 protein levels was prevented by the proteasome inhibitor bortezomib, suggesting that DNA damage resulted in ubiquitination and proteasomal degradation of NKX3.1.

We investigated the relationship between NKX3.1 binding to ATM, (S/T)Q site phosphorylation, and NKX3.1 degradation. We expressed either ATM or ATM(Δ431–490) in 293T cells along with MYC-NKX3.1. After UV exposure of cells preloaded with BrdU and treated with Hoechst 33258 dye p(S/T)Q phosphorylation of NKX3.1 was seen in the presence of exogenous ATM,

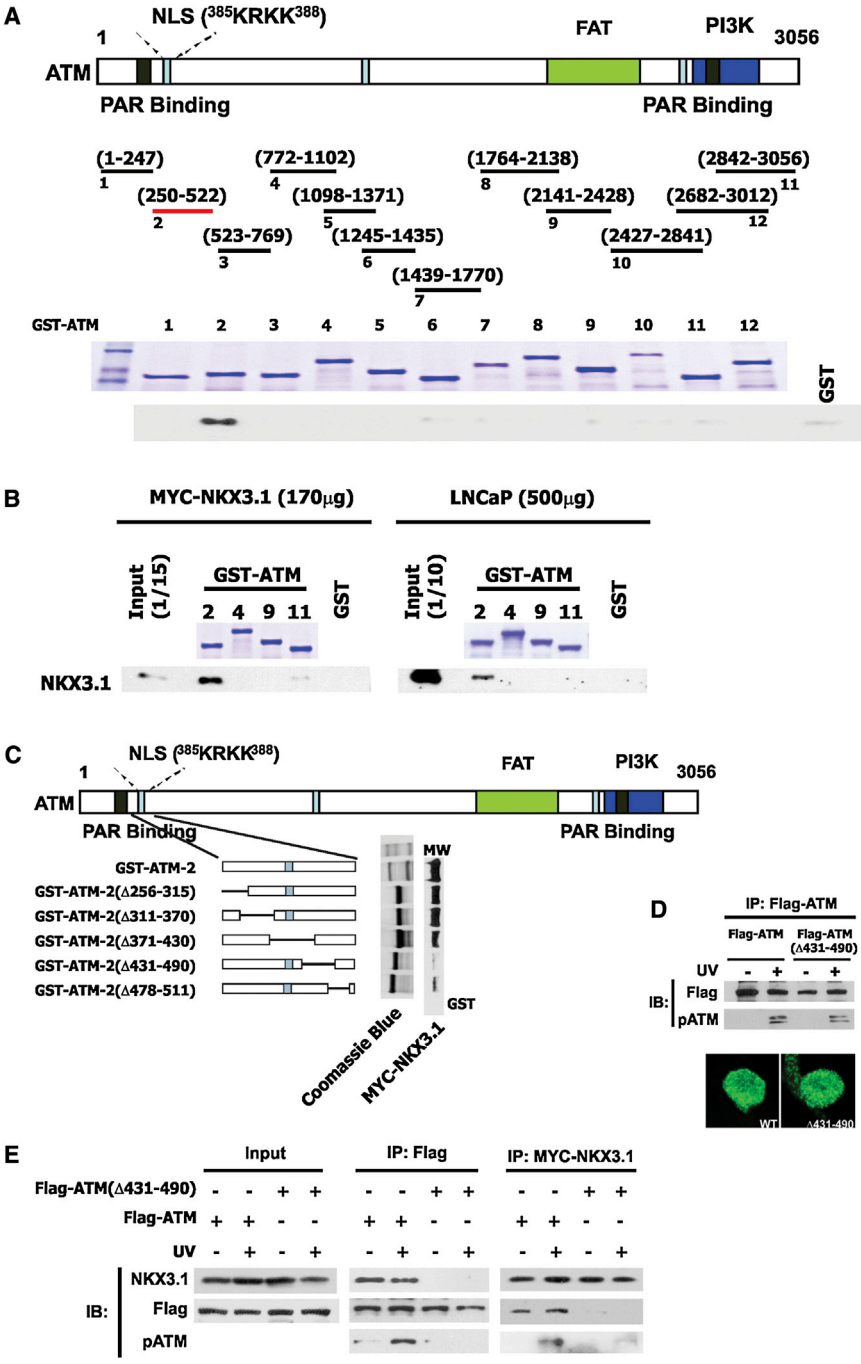

Figure 3. NKX3.1 Binding to ATM

(A) GST fusion proteins from different regions of ATM as shown in the upper panel were produced and resolved on SDS-PAGE stained with Coomassie blue. A pull-down assay was performed with 20 μl of bead slurry containing GST-ATM fusion peptides incubated with purified His-NKX3.1. Glutathione beads bound to fusion protein were incubated, washed four times, and subjected to immunoblotting with NKX3.1 antiserum.

(B) Lysate from 293T cells expressing MYC-NKX3.1 or LNCaP cells was subjected to GST pull-down with the four fusion peptides as indicated. GST-alone control lanes are shown as indicated.

(C) GST-ATM-2 was sequentially deleted with a Site-Directed Mutagenesis Kit (Stratagene). PCR was performed as described by the manufacturer except with an extension time of 1.5 kb/min for 35 cycles. A GST pull-down assay was performed with 200 μg of 293T(MYC-NKX3.1) cell lysates.

(D) 293T cells engineered to express Flag-ATM or Flag-ATM(Δ431-490) were preloaded with BrdU and pretreated with Hoechst 33258 dye prior to exposure to 10 mJ/cm^2 UV. Cell lysates were subjected to immunoprecipitation and immunoblotting as shown. Also, in the lower panels, expression of nuclear Flag-ATM constructs was demonstrated by immunofluorescence.

(E) 293T cells engineered to express MYC-NKX3.1 and Flag-ATM constructs were preloaded with BrdU and pretreated with Hoechst 33258 dye prior to exposure to UV irradiation. The cells were harvested 10 min after UV exposure. Immunoprecipitations were performed with Flag antibody-bound agarose (Sigma) or MYC antibody (Santa Cruz) with a Catch-Release Kit (Millipore). Immunoblots were probed with antibodies as indicated.

See also Figure S2.

but not exogenous ATM(Δ431–490) (Figure 4C, upper panel). In Figure 4C the Flag epitope tag is used to demonstrate expression levels of the ATM transgenes. Moreover, reduced cellular levels of MYC-NKX3.1 after UV exposure were seen in the presence of ATM, but not ATM(Δ431–490) (Figure 4C, immunoblots in lower panel), thus demonstrating a correlation among NKX3.1 binding to ATM, (S/T)Q phosphorylation, and NKX3.1 degradation after UV exposure. A similar effect was seen on MYC-NKX3.1 when endogenous ATM in 293T cells was knocked down with ATM siRNA (Figure 4D). ATM knockdown was associated both with reduced (S/T)Q phosphorylation of NKX3.1 (Figure 4D, upper panel) and with persistence of cellular NKX3.1 after UV exposure (Figure 4D, lower panel). In addition, we demonstrated that both wild-type and kinase-dead (KD) ATM associated with NKX3.1, but no (S/T)Q phosphorylation was seen with KD ATM, further demonstrating that NKX3.1 is an ATM substrate (Figure 4E).

NKX3.1 Binding Domain for ATM

The suggestion that NKX3.1 was a substrate for ATM and that NKX3.1 (S/T)Q phosphorylation led to NKX3.1 degradation implied that ATM and NKX3.1 are involved in a regulatory loop wherein NKX3.1 activates ATM, which in turn phosphorylates NKX3.1, leading to its degradation. To explore this interaction

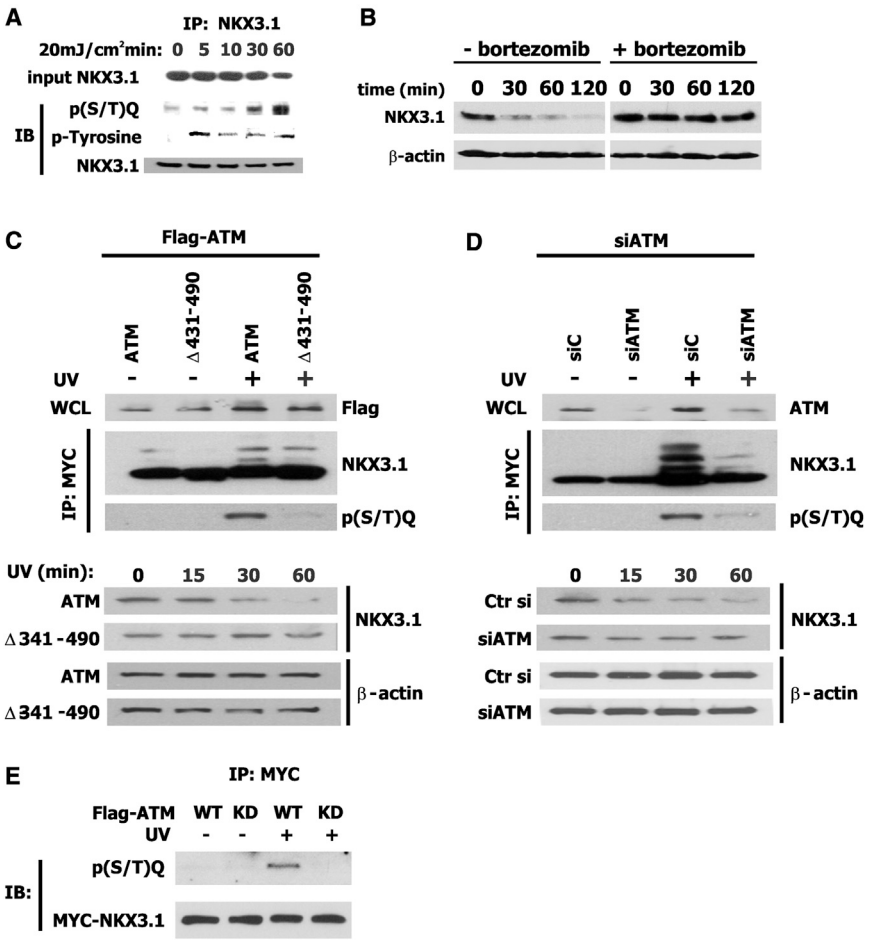

Figure 4. DNA Damage Induces Posttranslational Modification of NKX3.1

(A) LNCaP cells pretreated with BrdU and Hoechst 33258 dye were harvested after 20 mJ/cm^2 UV irradiation. The 500 μg nuclear extract was incubated with 4 μg of either IgG or goat anti-NKX3.1 antibody (Santa Cruz) together with Catch-Release affinity ligand and columns. Eluted protein was resolved by SDS-PAGE and immunoblotted as shown.

(B) LNCaP cells were preloaded with BrdU and pretreated with Hoechst 33258 dye with or without 100 nM bortezomib for 1 hr prior to exposure to 10 mJ/cm^2 UV irradiation. Samples were harvested and immunoblotting was done with NKX3.1 antiserum.

(C) 293T cells were engineered to express Flag-ATM constructs and MYC-NKX3.1. Cells were preloaded with BrdU and pretreated with Hoechst 33258 dye prior to 10 mJ/cm^2 UV exposure. Cells were collected 60 min after UV exposure and lysates were subjected to immunoprecipitation and immunoblotting (upper panel) or immunoblotting (lower panel). For immunoprecipitation, bortezomib was added 30 min prior to irradiation.

(D) The same as in (C) except that control and ATM knockdown vectors were transfected into 293T cells.

(E) 293T cells transfected with Flag-ATM expression plasmids and MYC-NKX3.1 were preloaded with BrdU and pretreated with Hoechst 33258 dye prior to 10 mJ/cm^2 UV irradiation. Cells were harvested 30 min after irradiation. Lysates were subjected to immunoprecipitation with MYC antibody and immunoblotting.

further, we determined the domain(s) of NKX3.1 that are responsible for ATM binding. Using GST-ATM-2 as a binding substrate for epitope-tagged NKX3.1 peptides, we showed that the homeodomain was both necessary and sufficient for binding (114–208 peptide in Figure 5A) and that the peptide N-terminal to the homeodomain did not bind ATM-2 (1–123 peptide in Figure 5A). In a more detailed deletion analysis of the NKX3.1 homeodomain, we observed that the regions spanning amino acids 131–140 and 151–160 both influenced ATM binding (Figure 5B). These regions encompass T134 and are adjacent to T166, two candidate TQ ATM phosphorylation sites.

When the native NKX3.1 was incrementally truncated from the C-terminal end, we observed a marked reduction in binding affinity (see the five peptides illustrated on the right of Figure 5A). This suggested that the C-terminal domain was permissive for binding to the ATM-2 peptide. We found that the NKX3.1 C-terminal domain had a significant influence on ATM binding and also on the functional interaction between NKX3.1 and ATM. Loss of the single C-terminal tryptophan of NKX3.1 markedly diminished ATM binding, and deletion of 225–234 abrogated binding (Figure S2A). Interestingly, restoration of tryptophan to NKX3.1(1–224) restored the ability to bind ATM-2, suggesting that the C-terminal tryptophan played an important role in facilitating ATM binding (Figure S2B). Loss of the C-terminal domain abrogated the effect of NKX3.1 on ATM activation by the MRN complex (Figure S2C), in contrast to the effect seen with the full-length NKX3.1 (Figure 2E). However, the NKX3.1(1–183) peptide was fully competent to enhance ATM activation by H_2O_2 (Figure S2D). Thus, we were able to discriminate between the stronger effect of NKX3.1 on ATM activation by H_2O_2 and the effect on ATM activation by the MRN complex by deletion analysis of NKX3.1.

Since we had demonstrated that (S/T)Q phosphorylation was important for NKX3.1 turnover after DNA damage, and that ATM bound to the homeodomain between the two TQ sites, we next demonstrated that both homeodomain T(134)Q and T(166)Q dipeptides are in fact phosphorylated by ATM. As a first step, we engineered a compound mutation of each of two of all three candidate ATM phosphorylation sites, S48, T134, and T166. Each of these amino acids in NKX3.1 precedes a Q, thus providing SQ or TQ sites preferred as targets for ATM phosphorylation. Whereas loss of S48 did not affect (S/T)Q phosphorylation after DNA damage, the compound mutation T134,166A abrogated (S/T)Q phosphorylation of NKX3.1 (Figure 5C). The timing of TQ dipeptide phosphorylation that is abrogated by T134A/T166A was consistent with the result shown in Figure 4A, such that TQ phosphorylation was seen at 30 min predominantly at T134 and at 60 min at both T134 and T166 (Figure 5D).

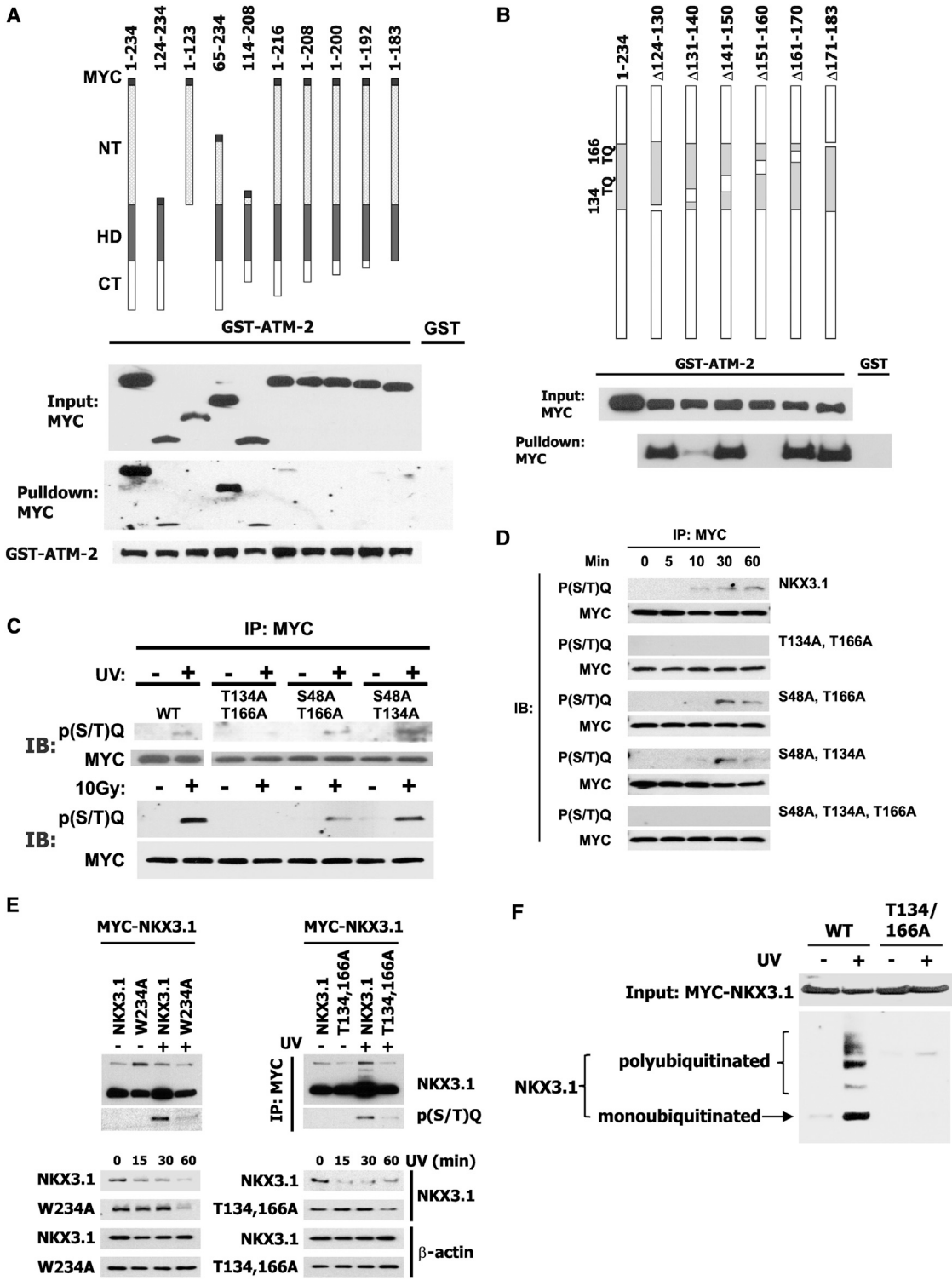

Figure 5. ATM Binding Domains in NKX3.1

(A) Glutathione-bead-bound GST-ATM-2 peptide was incubated with cellular extract of 293T cells that had been transfected with MYC-NKX3.1 constructs as shown at the top of the panel. Bound MYC-NKX3.1 peptides were detected by immunoblotting.

(B) The same experiment as in (A), but with constructs containing deletions of the NKX3.1 homeodomain.

(C) LNCaP cells transfected with MYC-NKX3.1 constructs preloaded with BrdU and pretreated with Hoechst 33258 dye and bortezomib were harvested 1 hr after 10 mJ/cm^2 UV irradiation. Cell lysates were subjected to immunoprecipitation with MYC antibody and then analyzed by immunoblotting.

(legend continued on next page)

Moreover, binding of NKX3.1 to ATM was required for degradation, as missense mutation of the terminal NKX3.1 tryptophan abrogated TQ phosphorylation and prolonged the half-life of NKX3.1 after DNA damage (Figure 5E, left panels). The effect on both TQ phosphorylation and the NKX3.1 half-life of the NKX3.1(W234A) missense mutation was the same as the effect of changing both T134 and T166 to alanines (Figure 5E). Therefore, binding NKX3.1 to ATM was required for both substrate interaction and DNA-damage-induced turnover, implying that ATM played a role in modulating the effect of NKX3.1 after DNA damage. Lastly, phosphorylation of NKX3.1 at the homeodomain TQ sites was shown to be important for DNA-damage-induced ubiquitination of NKX3.1, demonstrating that ATM phosphorylation resulted in proteasomal degradation of NKX3.1 during the first hour after DNA damage (Figure 5F).

Even though threonines 134 and 166 were substrate sites for ATM kinase, we also wanted to examine how these sites influence the effect of NKX3.1 on ATM function. We restored NKX3.1 expression in LNCaP(si471) cells with either wild-type or NKX3.1(T134,166A) expression constructs. The loss of both threonines resulted in a 40% reduction in the intensity of γH2AX to a DNA damage site (Figure S3A) and delayed activation of ATM phosphorylation (Figure S3B). We should point out that the effect of T→A mutations at these two sites may have changed the homeodomain sufficiently to compromise binding with ATM, and the attenuation of NKX3.1's effect on ATM activity may not have been due to the loss of the substrate target sites per se.

Tyrosine Phosphorylation of NKX3.1

We showed that NKX3.1 underwent tyrosine phosphorylation within minutes of DNA damage (Figure 4A). To determine whether tyrosine phosphorylation of NKX3.1 was important to initiate its participation in the DNA damage response, we first identified the target tyrosine phosphorylation site(s). Using comprehensive site-directed mutagenesis of all tyrosines in NKX3.1, we found that Y222 in the C-terminal domain was the site for tyrosine phosphorylation after DNA damage. In particular, mutation of tyrosine 222 to phenylalanine (Y222F) was as effective as mutation of all NKX3.1 tyrosines to phenylalanine residues in attenuating the effect of DNA damage on degradation of NKX3.1. Conversely, an NKX3.1 protein with native Y222 but all other tyrosines mutated to phenylalanine retained the effect of DNA damage on NKX3.1 protein levels (Figure 6A). The importance of Y222 in the response of NKX3.1 to DNA damage was further demonstrated by the loss of DNA-damage-induced tyrosine phosphorylation of NKX3.1 when tyrosine 222 was mutated to phenylalanine, and by the preservation of tyrosine phosphorylation in the NKX3.1 derivative in which all tyrosines except Y222 were mutated to phenylalanine (Figure 6B). Also, Y222 was shown to be required for optimal NKX3.1 binding with ATM. In physical association experiments with GST-ATM-2, the preservation of only Y222 resulted in the same degree of binding to ATM as the native NKX3.1 protein, whereas loss of only Y222 diminished NKX3.1 association with the ATM peptide after irradiation (Figure 6C). Loss of Y222 reduced the association of NKX3.1 with endogenous ATM in 293T cells, comparable to the effect of loss of the two threonine phosphorylation sites in the homeodomain. The same DNA damage conditions used for 293T cells caused association of endogenous NKX3.1 and ATM in LNCaP cells (Figure 6D).

Importantly, tyrosine 222 phosphorylation had a functional role in the DNA damage response. Tyrosine 222 was necessary for efficient activation of ATM kinase by NKX3.1. Exogenous expression of NKX3.1, but not NKX3.1(Y222F), in 293T cells activated ATM phosphorylation of P53 (Figure 6E). Moreover, compared with native NKX3.1, NKX3.1(Y222F) expression in LNCaP(si471) cells was accompanied by marked attenuation in recruitment of γH2AX to a DNA damage site (Figure 6F). Having previously shown that NKX3.1 expression enhanced colony-forming ability after DNA damage (Bowen and Gelmann, 2010), we compared the capacities of NKX3.1(Y222F) and the wild-type protein to affect cell survival in a colony-formation assay. We engineered 293T cells to express NKX3.1 along with a GST coselectable marker. Colony formation was assayed after two different doses of UV in BrdU-loaded and Hoechst 33258 dye-treated cells and in cells exposed to 5 and 10 Gy γ-irradiation. In each instance, NKX3.1(Y222F) was attenuated compared with the wild-type in enhancing cell survival (Figure 6G). In LNCaP prostate cancer cells, we also observed that NKX3.1(Y222F) was attenuated in its ability to affect cell survival after DNA damage induced both by UV and by γ-irradiation (Figure S4). Therefore, Y222 phosphorylation of NKX3.1 after DNA damage facilitated the interaction and activation of ATM, demonstrating that NKX3.1 is a recipient of signal transduction early in the DNA damage response and potentiates ATM activation.

An important consequence of the role of NKX3.1 in DNA repair is the effect of the protein on *TMPRSS2-ERG* rearrangement (C.B. and E.P.G., unpublished data). NKX3.1 can be found at the break points in the *ERG* gene that recombine with *TMPRSS2* to form the fusion transcripts found in the majority of prostate cancers (Tomlins et al., 2005). Reduced levels of NKX3.1 predispose cells to *TMPRSS2-ERG* rearrangement that is mediated by androgen receptor (Mani et al., 2009; Figure 6H, left panel). Moreover, NKX3.1 recruits ATM to a major locus of *ERG* gene

(D) Experiment performed as in (C), but with cells harvested at the indicated time points.
(E) 293T cells expressing MYC-NKX3.1 constructs were preincubated with BrdU, Hoechst 33258 dye, and bortezomib (upper panels) prior to 10 mJ/cm^2 UV irradiation. Cells were harvested 60 min after irradiation and subjected to immunoprecipitation with MYC antibody and then immunoblotting. The lower panels show levels of NKX3.1 after irradiation from cultures that were not treated with bortezomib.
(F) LNCaP cells were cotransfected with expression constructs for a fusion HIS-ubiquitin peptide and either epitope tagged MYC-NKX3.1 or MYC-NKX3.1 (T134/166A). They were then preloaded with BrdU and pretreated with Hoechst 33258 dye ± 100 nM bortezomib for 1 hr, followed by exposure to 10 mJ/cm^2 UV irradiation. Cells were harvested 4 hr after UV exposure. A His Bind Purification Kit (Novagen) was used to assess the ubiquitination of NKX3.1. Eluted proteins were resolved by SDS-PAGE and immunoblotted with polyclonal anti-MYC antibody.
See also Figures S2 and S3.

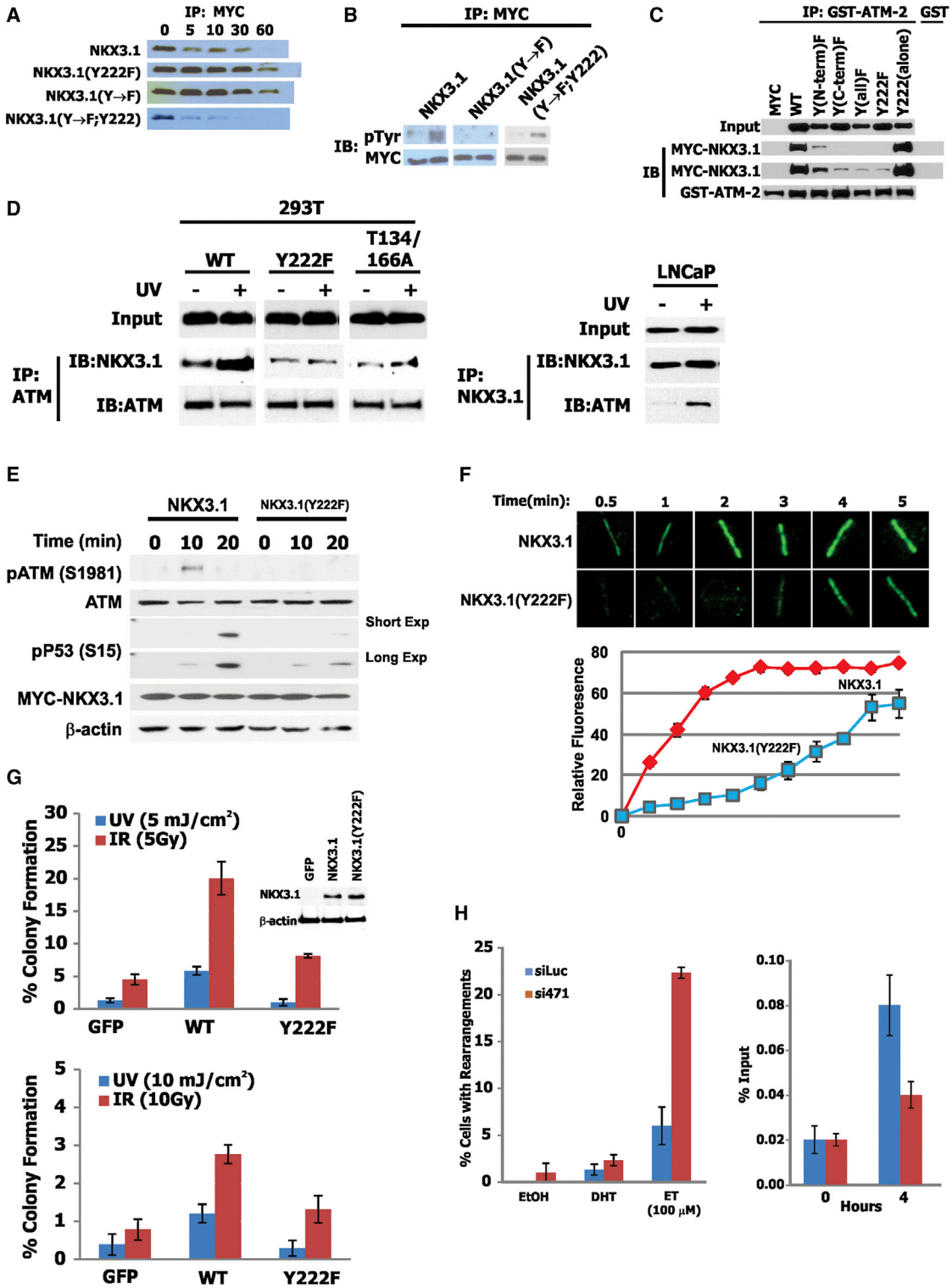

Figure 6. Tyrosine Phosphorylation of NKX3.1 Induced by DNA Damage

(A) 293T cells transfected with Flag-ATM expression plasmids and MYC-NKX3.1 expression constructs were preincubated with BrdU and Hoechst 33258 dye prior to 10 mJ/cm^2 UV irradiation. Cells were harvested 30 min after irradiation. Lysates were subjected to immunoprecipitation with MYC antibody and immunoblotting. (B) LNCaP cells were transfected with MYC-NKX3.1 constructs. Cells were preloaded with BrdU, pretreated with Hoechst 33258 dye and 100 nM bortezomib, and harvested 5 min after exposure to 10 mJ/cm^2 UV irradiation. The cell lysates were subjected to immunoprecipitation with MYC antibody and immunoblotted with either antibody to MYC or phosphotyrosine.

(legend continued on next page)

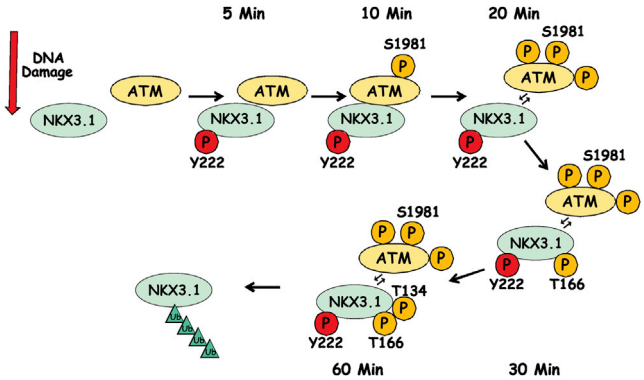

Figure 7. Proposed Model for NKX3.1 Interaction with ATM

Within minutes of DNA damage, ATM is phosphorylated on S1981 and NKX3.1 on tyrosine 222. Both posttranslational modifications facilitate binding of the two proteins, which results in activation of ATM activity and accumulation of pATM at sites of DNA damage. By 30 min, ATM phosphorylates NKX3.1 on T166 and then T134, resulting in NKX3.1 ubiquitination and degradation resulting from an apparent regulatory interaction.

fusion (Lin et al., 2009), and that recruitment is attenuated in LNCaP(si471) cells (Figure 6H, right panel). This result and results yet to be published demonstrate that the effect of NKX3.1 on the DNA repair response plays a role in the earliest steps of prostate carcinogenesis by influencing the propensity for *TMPRSS2-ERG* rearrangement.

DISCUSSION

Clinical prostate cancer occurrence rises more sharply (>7-fold) than any other cancer during the last three decades of life. In the aging prostate and the inflamed gland, two conditions that predispose to prostate cancer, NKX3.1 is downregulated (Bethel et al., 2006; Khalili et al., 2010). NKX3.1 modulates the response to DNA damage (Bowen and Gelmann, 2010) by interacting and upregulating ATM activation, as we have now shown. The effect of NKX3.1 on the DNA repair process has important implications for the etiology, prevention, and treatment of prostate cancer. As an early event in primary prostate cancer and PIN, *NKX3.1* haploinsufficiency and methylation represent major contributors to prostate carcinogenesis at this early preinvasive stage (Asatiani et al., 2005; Bethel et al., 2006). Furthermore, early loss of *NKX3.1* and downregulation of NKX3.1 protein expression contribute to the susceptibility of prostate epithelial cells to oxidative damage, both in human prostate cancer (Nelson et al., 2003) and in mouse models (Ouyang et al., 2005). These effects are exacerbated by decreased expression of *GSTP1* (Lin et al., 2001) and also may be affected by mutations in the *macrophage scavenger receptor 1* (Nupponen et al., 2004; Seppälä et al., 2003; Wang et al., 2003). Our recent studies have now established a probative link between NKX3.1 loss and the DNA damage response (Bowen and Gelmann, 2010), which may help explain its functions in tumor suppression.

From the data in this paper, we have derived a model of NKX3.l action in response to DNA damage (Figure 7). Within 5 min of DNA damage, NKX3.1 undergoes phosphorylation at tyrosine 222 by an as yet unidentified kinase. Tyrosine phosphorylation is required for NKX3.1 to associate with ATM in the region between amino acids 431 and 490. NKX3.1 binds to ATM via the homeodomain and also via the C-terminal domain, and binding is enhanced by a C-terminal tryptophan. NKX3.1 binding to ATM is favored by early phosphorylation of ATM, as shown at the 10 min time point in Figure 5C. Therefore, we suggest that NKX3.1 binding to ATM is modulated by ATM phosphorylation that occurs at many sites during the DNA damage response. By 30 min, ATM initiated phosphorylation of two threonines that flank the ATM binding site in the NKX3.1 homeodomain. Threonine 166 appears to be phosphorylated first, followed by threonine 134. Phosphorylation at these two sites mediates ubiquitination and DNA-damage-induced proteasomal degradation of NKX3.1, thus terminating NKX3.1's involvement in the damage response.

Based on our recent findings, we propose that a principal mechanism by which NKX3.1 loss affects prostate carcinogenesis is via impaired DNA damage signaling. Many of the histologic and pathologic changes in the aging prostate are

(C) GST-ATM-2 peptide bound to glutathione beads was incubated with cellular extract of 293T cells transfected with MYC-NKX3.1 constructs as shown. Input and peptide-bound NKX3.1 were detected by immunoblotting with anti-MYC antibody. At the right is shown the negative control using GST not fused to ATM-2.
(D) 293T were transfected with MYC-NKX3.1 expression constructs. Cells were preloaded with BrdU and pretreated with Hoechst 33258 dye and 10 nM bortezomib for 30 min prior to exposure to 10 mJ/cm^2 UV irradiation. Lysates were subjected to immunoprecipitation with 2 μg anti-ATM antiserum (Santa Cruz) and immunoblotted with NKX3.1 antiserum or monoclonal ATM antibody (GeneTex). LNCaP cells were similarly treated without transfection.
(E) 293T cells expressing MYC-NKX3.1 constructs by transient transfection were pretreated with BrdU and Hoechst 33258 dye prior to 10 mJ/cm^2 UV exposure. The cells were collected at the indicated times after irradiation and processed for immunoblotting.
(F) LNCaP(si471) cells were transiently transfected with MYC-NKX3.1 constructs as shown. Cells were pretreated with BrdU and Hoechst 33258 dye followed by LMI (speed: 20; focus: 63; power: 36) at the indicated times. Cells were fixed and stained with gH2AX monoclonal antibody. The relative intensity of γH2AX accumulation was measured with ImageJ software by counting 30 cells per time point.
(G) 293T cells were transfected with the indicated NKX3.1 expression constructs and the selectable GFP expression plasmid. Cells were preloaded with BrdU and pretreated with Hoechst 33258 dye. Cells were sorted by GFP with a BD FACSAria Cell Sorter and plated on poly-L-lysine-coated dishes for 4 hr before exposure to either 10 mJ/cm^2 UV or 10 Gy γ-irradiation. Colony formation was counted 7–10 days after treatment. The percentage of colony formation was obtained by normalization to untreated control samples. The inset immunoblot demonstrates equivalent expression of transgenes in the transfected cells.
(H) LNCaP(siLuc) and LNCaP(si471) cells were synchronized with 5 μM α-amanitin for 2 hr and exposed to EtOH or 100 nM DHT for 1 hr and then treated with 100 μM etoposide. Cells were harvested after 24 hr. FISH analysis was done to identify cells with TMPRSS2-ERG rearrangements. One hundred cells were analyzed and the data are derived from three independent experiments. Right panel: data from a ChIP assay performed with primers flanking the ERG IV break site (Lin et al., 2009). Extracts of cells treated with either EtOH or 100 μM DHT plus 100 μM etoposide for 4 hr were subjected to ChIP with ATM antibody (Santa Cruz). ATM binding at the break point was quantitated by ImageJ software and expressed as a percentage of input.
See also Figure S4.

accompanied by decreased NKX3.1 expression, thus predisposing to DNA damage and carcinogenesis. Even in the inflamed or aging prostate, NKX3.1 loss is mediated by inflammatory cytokines that induce phosphorylation of NKX3.1, leading to ubiquitination and proteasomal degradation, and thus shortening the protein's half-life (Markowski et al., 2008). The same inflammatory insult also increases the chance of mutation by oxidative DNA damage (Nelson et al., 2003; Ouyang et al., 2005). Oxidative damage is mediated to a large part by the formation of 8-oxo-guanine adducts that can cause mutational nucleotide transitions if they are not repaired (Grollman and Moriya, 1993). Repair of 8-oxo-guanine adducts is accomplished by base excision repair, which has been shown to be affected by ATM activation and CHK2 phosphorylation (Chou et al., 2008; Parlanti et al., 2002; Pascucci et al., 2002). ATM is likely to play a critical role in the cell's response to oxidative DNA damage, since the enzyme is activated by oxidation alone in the absence of damaged DNA (Guo et al., 2010b). We show in this paper that NKX3.1 augments ATM activation more profoundly in response to oxidation than to the presence of damaged DNA. Thus, an important function of NKX3.1 is to accelerate and amplify ATM activation in the prostate, a tissue that is subject to remarkably high levels of oxidative stress due to inflammation.

Our findings are also relevant to stem cell biology because the expression of NKX3.1 in the prostate stem cells known as castration-resistant Nkx3-1-expressing cells (CARNS) may increase stem cell survival by enhancing the cell's ability to repair DNA damage. The role of NKX3.1 in the stem cell may be further expanded to include cooperation with androgen receptor transcriptional activation (He et al., 2010). In fact, NKX3.1 often colocalizes with androgen receptor for transcriptional activation and helps to drive a survival program in prostate epithelial cells, suggesting yet another mechanism by which NKX3.1 expression may be very important for stem cells (Tan et al., 2012). The role of NKX3.1 in murine prostate stem cells may also be relevant for humans, as CARN-like cells have now been described in the human prostate (Germann et al., 2012).

NKX3.1 is expressed in very few human tissues beyond the prostate gland and in no tissues where its expression is present in the majority of cells (Bowen et al., 2000). Therefore, the effect of NKX3.1 on the DNA damage response and on cellular survival after DNA damage is largely specific to the prostate. NKX3.1 also activates topoisomerase I, and we have shown in gene-targeted mice that the effect of Nkx3.1 on topoisomerase I is localized only to the prostate gland (Bowen et al., 2007). Topoisomerase I is a ubiquitous DNA unwinding enzyme that is highly conserved in evolution and has been shown, among its many effects, to play a role in the cell's susceptibility to DNA damage (Miao et al., 2007). Thus, NKX3.1 enhances the activity of two key enzymes in the DNA repair process, affecting both the damage response via ATM and the capability for DNA repair via topoisomerase I.

We speculate that our findings suggest a biological explanation for differences observed in the sensitivities of different tissue types to γ-irradiation, and differences in their abilities to function after irradiation. Inherent in our findings is the implication that prostate-specific expression of NKX3.1 translates into tissue-specific effects on the DNA repair process. Thus, our work provides insight into the molecular mechanisms of tissue-specific differences of DNA repair, and perhaps radiation sensitivity. The efficacy of radiation therapy for the treatment of prostate cancer, as well as long-standing observations that there is a dose-response curve for radiation to provide long-term disease control, underscore the importance of finding ways to affect DNA repair pathways in prostate cancer cells (Pollack et al., 2000; Pollack and Zagars, 1997).

EXPERIMENTAL PROCEDURES

Cell Culture, Transfection, and Reagents

LNCaP, 293T, and PC-3 cell culture and transfection, as well as the LNCaP derivative lines with NKX3.1 knockdown, LNCaP(siLuc), and LNCaP(si471) have been previously described (Bowen and Gelmann, 2010). ATM and ATR inhibitors Ku55933 and caffeine were purchased from Sigma. Cycloheximide was obtained from Sigma. Control inhibitory RNA and siATM SMARTpool siRNAs were obtained from Dharmacon. 293T cells were engineered for stable incorporation of pHPRT-DP-GFP (SceGFP) plasmid (from Maria Jasin) with lipofectamine 2000 (Rouet et al., 1994). The cells were transfected with pcDNA3-NKX3.1 and pCBASce, an I-SceI expression vector, for 24 hr. ChIP was performed with 2 μg of anti-NKX3.1 antibody (goat; Santa Cruz). The PCR primers were GFP 1F:5′- CGT CCA GGA GCG CAC CAT CTT CTT-3′ and GFP 1R:5′-ATC GCG CTT CTC GTT GGG GTC TTT-3′.

Constructs

GST-ATM fusion peptide expression constructs were provided by K.K. Khanna (University of Queensland, Brisbane, Australia). The GST-P53 expression vector was obtained from T.T.P. Wild-type and KD Flag-ATM vectors were provided by M.B. Kastan (St. Jude Children's Research Hospital, Memphis, TN, USA). GST-ATM2 deletion constructs were produced using the QuikChange site-directed mutagenesis kit (Stratagene). Flag-ATM(Δ431-490) was generated with the QuikChange XL site-directed mutagenesis kit (Stratagene) with a modified protocol, with the PCR extension time at 1.5 min/kb. pcDNA3-NKX3.1 full-length and truncated constructs was produced by inserting PCR fragments of NKX3.1 into pcDNA3 vector at EcoRI and *XhoI* sites. MYC-NKX3.1 HD and C terminus deletion constructs were made by introducing NKX3.1 PCR fragments into pCMV-MYC vector at EcoRI and *Xho I* sites. The MYC-NKX3.1 point mutant or combined point and deletion mutant constructs were generated either by mutation with the QuikChange site-directed mutagenesis kit or by inserting modified PCR fragments into pCMV-MYC vector. GST-p53 substrate (pTP317; 1–102 aa) was provided by T.T.P.

Induction of DNA Damage

In most experiments, double-stranded DNA breaks were introduced by irradiating cells with 20 mJ/cm^2 after 48 hr of preloading with 10 μM BrdU and a 30 min treatment with 10 μg/ml Hoechst 33258 dye (Limoli and Ward, 1993). This approach has been used by other groups and validated as a method to induce double-stranded DNA breaks (Huang et al., 2004; Khalil et al., 2011). Key experiments were repeated with γ-irradiation. We previously showed that NKX3.1 has affects equal to the DNA damage response induced by γ-irradiation, mitomycin C, and UV without cell sensitization (Bowen and Gelmann, 2010).

Protein Purification

His-NKX3.1 was prepared as previously described (Bowen et al., 2007). The MRN complex and GST-p53 substrate were purified as previously described (Bhaskara et al., 2007; Lee and Paull, 2004). Dimeric ATM was made by transient transfection of expression constructs into HEK 293T cells using calcium phosphate and purified as previously described (Lee and Paull, 2006). Protein concentrations were determined by quantification of protein preparations with standards on colloidal Coomassie-stained SDS-PAGE gels using the Odyssey system (Li-Cor).

Immunofluorescence and LMI

Cells were fixed and permeabilized in CSK buffer (10 mM PIPES, 100 mM NaCl, 300 mM sucrose, 3 mM $MaCl_2$, and 1 mM EGTA) containing 4% formaldehyde and 0.1% Triton X-100 for 15 min, and LMI was performed as previously described (Bowen and Gelmann, 2010). Cells were sensitized with 10 μg/ml of Hoechst dye 33258 for 30 min. Prior to irradiation, cells were washed twice with culture medium. Irradiation was performed through a 40× objective with a cut speed ranging from 10% to 40% and power output of 45%, focus 61. Operation was assisted by the PALM Robo-Software supplied by the manufacturer. Cells were fixed and permeabilized in CSK buffer (10 mM PIPES, 100 mM NaCl, 300 mM sucrose, 3 mM $MgCl_2$, 1 mM EGTA) containing 4% formaldehyde and 0.1% Triton X-100 for 15 min. The following procedure was then performed as previously described (Bowen and Gelmann, 2010): primary γH2AX and NKX3.1 antibodies were employed at dilutions of 1:1,000 or 1:200, respectively, and samples were incubated with secondary antibodies γH2AX (FITC, goat anti-mouse immunoglobulin G [IgG]; Vector) and NKX3.1 (Alexa Fluor-568, goat anti-rabbit IgG; Molecular Probes).

Immunoprecipitation and Immunoblotting

Cell lysates were prepared with RIPA buffer containing protease inhibitors (cOmplete, Mini; Roche) and with phosphatase inhibitors when appropriate (PhosStop; Roche). Immunoprecipitation was done with 500 μg of cell lysate and 2 μg of antibody followed by the use of the Catch and Release Immunoprecipitation kit (Millipore) or protein A/G agarose (Calbiochem). Proteins were resolved by SDS-PAGE, transferred to a nitrocellulose membrane, immunoblotted, and detected with SuperSignal West Pico Chemiluminescent Substrate (Thermo Scientific) or SuperSignal West Dura Extended Duration Substrate (Thermo Scientific). The antibodies used were as follows: γH2AX (Upstate), pATM-S1981 (Rockland), ATM (GeneTex), ATR (C-19; Santa Cruz), β-actin (Sigma), H2AX antiserum (Abcam), phospho-P53(S15) (Cell Signaling), Flag (Sigma), p(S/T)Q (Cell Signaling), and phosphotyrosine and MYC (Santa Cruz).

GST Pull-Down Assay

GST fusion peptides were expressed in BL21 cells after induction by 0.2 mM isopropyl β-D-1-thiogalactopyranoside for 2–3 hr. Cells were harvested and resuspended in STE buffer (10 mM Tris [pH 8.0], 150 mM NaCl, and 1 mM EDTA), followed by addition of freshly prepared lysozyme and then incubation on ice for 15 min. Just before sonication, 1 M dithiothreitol (DTT) and 10% sarkosyl were added. The lysate was cleared by centrifugation, incubated with 10% Triton X-100 in STE buffer for 30 min, and equilibrated glutathione beads. Where indicated, 100–250 ng of purified His-NKX3.1 or 250–500 μg of LNCaP cell lysate was incubated with agarose-bound GST-fusion peptides for 1 hr at room temperature. Dissociation was achieved with SDS, and proteins were resolved on SDS-PAGE and detected by immunoblotting.

ATM Kinase Assay

FLAG-tagged ATM and KD ATM constructs were expressed by transfection. Cells were lysed with TGN buffer (50 mM Tris [pH7.4], 150 mM NaCl, 10% glycerol, 0.2% Tween 20, 0.2% NP40, and 1 mM DTT), protease inhibitors, and phosphatase inhibitors. Epitope-tagged proteins were isolated from 100 μg of lysate with 30 μl of anti-FLAG M2 agarose (Sigma-Aldrich) in TGN buffer for 1 hr at 25°, washed three times with TGN containing 0.5 M LiCl, and then washed once with kinase buffer. GST-P53 fusion proteins were expressed in *Escherichia coli* BL2 and affinity purified. ATM kinase assays were done in kinase buffer (10 mM HEPES [pH7.5], 50 mM NaCl, 10 mM $MgCl_2$, 10% glycerol, and 500 μM ATP). Agarose-bound Flag-ATM and His-NKX3.1 were mixed at 25°C for 30 min, and then 1 μg of GST-P53 was added and incubated at 30°C for 60 min in a volume of 30 μl. GST-P53 was resolved by SDS-PAGE, followed by immunoblotting with monoclonal phospho-P53(S15) and NKX3.1 antiserum.

In Vitro ATM Kinase Assay

ATM kinase assays contained 0.7 nM dimeric ATM, 5 nM GST-p53 substrate, 1.5 nM MRN complex, 10 ng DNA, and varying amounts of NKX3.1 as indicated in the figure legends. Kinase assays were performed in kinase buffer (50 mM HEPES [pH 7.5], 50 mM potassium chloride, 5 mM magnesium chloride, and 10% glycerol, 1 mM ATP, and 1 mM DTT) for 90 min at 30°C in a volume of 40 μl as described previously (Lee and Paull, 2005). In experiments where H_2O_2 was used, no additional DTT was added to the reactions and ATM kinase assays were performed with 40 nM P53 and 0.7 mM H_2O_2 as previously described (Guo et al., 2010b). Phosphorylated p53 (ser15) was detected as previously described (Lee and Paull, 2004) using phospho-specific antibody from Calbiochem (PC461).

Fluorescence In Situ Hybridization

LNCaP(siLuc) and LNCaP(si471) cells were cultured in 35 mm dishes in phenol red-free Iscove's modified Eagle's medium (IMEM) containing 10% fetal bovine serum (FBS). To increase the frequency of chromosomal rearrangement, cells were treated with 100 μM etoposide after exposure to 100 μM dihydrotestosterone (DHT). Interphase cells were prepared for fluorescence in situ hybridization (FISH) analysis by 0.075 M KCl hypotonic treatment at 37°C for 30 min and fixed with 3:1 methanol:glacial acetic acid at 4°C.

FISH was performed 24 hr after fixation using BAC DNA probes labeled with biotin (Biotin-Nick Translation Mix; Roche) and digoxigenin (Dig-Nick Translation Mix; Roche). BAC DNA plasmids (BACPAC Resources Center, Children's Hospital, Oakland Research Institute) were amplified and purified using the QIAGEN Plasmid Midi Kit. To assay *TMNPRSS2-ERG* rearrangements, we used an *ERG* split probe that contains 5′*ERG* (DIG) (RP11-95I21) and 3′ *ERG* (BIO) (RP11-476D17). Prior to hybridization, the slides were pretreated with 2× SSC at 37°C for 15 min and then with 2× SSC at 75°C for 5 min, followed by passage through sequential washes of 70%, 80%, 95%, and 100% ethanol. Probes and slides were denatured at 75°C for 5 min separately with slides in prewarmed 70% formamide in 2× SSC. Hybridization was allowed to proceed at 37°C overnight. Posthybridization washes were performed in prewarmed 50% formamide in 2× SSC at 37° three times, followed sequentially by two washes in prewarmed 0.5× SSC/0.3% NP-40 solution, at 60°C for 2 min, one wash in 2× SSC/0.1% NP-40 at room temperature, and one wash in 1× PBS containing 0.1% Tween 20. Finally, the slides were incubated with 100 μl of blocking reagent (CAS block; ZYMED) with 1% goat serum 30 min at 25°C. FISH signals were detected with streptavidin Alexa Fluor 594 conjugate (Invitrogen) and anti-digoxigenin fluorescein antibodies (Roche) diluted in blocking reagent for 30 min at 25°C. Slides were counterstained with DAPI in PBS and mounted in Antifade Mounting Medium (Molecular Clones). Fluorescence images were captured with a 100× objective on an Axiovert wide-field microscope. Image analysis was done using ImageJ processing software.

TMPRSS2-ERG ChIP

Cells were grown to 70% confluence in phenol-red-free modified IMEM supplemented with 10% FBS, after which the medium was changed to IMEM with 10% charcoal-stripped FBS (CCS) for 3 days. Following the addition of 100 nM DHT for 60 min, cells were treated with 100 μM etoposide for 4 hr. Cells were subjected to crosslinking with 0.75% formaldehyde at 25°C for 8 min with agitation, the reaction was quenched with 125 mM glycine for 5 min, and the cells then were rinsed with ice-cold PBS twice. To prepare crude nuclei, cells were resuspended in hypotonic lysis buffer (20 mM Tris-HCl [pH 7.5], 10 mM NaCl, and 3 mM $MgCl_2$) with a protease inhibitor cocktail (Roche) on ice for 10 min. The nuclei were subjected to dounce homogenization with 20 strokes, suspended in RIPA buffer, and sonicated at output level 4, 15 times for 10 sec each at 1 min intervals on ice using a Micromix sonicator 3000. A ChIP assay was performed with 50 μg of chromatin DNA per reaction. Supernatants were collected and diluted 1:5 in buffer (1% Triton X-100, 2 mM EDTA, 150 mM NaCl, and 20 mM Tris-HCl [pH 8.1]), and 1% chromatin was used as the input sample. One milliliter of lysate was precleared with 10 μg sheared salmon sperm DNA (Invitrogen), 10 μl serum, and protein A-sepharose (50 μl of 50% slurry in 10 mM Tris-HCl [pH 8.1], 1 mM EDTA) for 1–2 hr at 4°C. Immunoprecipitation was performed overnight at 4°C with 2 μg antibody. After immunoprecipitation, 30 μl of protein A-Sepharose, 10 μg of salmon sperm DNA, and 10 μl of serum were added and the incubation was continued for 1–2 hr at 4°C. Precipitates were washed sequentially for 5 min each in TSE I (0.1% SDS, 1% Triton X-100, 2 mM EDTA, 20 mM Tris-HCl [pH8.1], and 150 mM NaCl), TSE II (0.1% SDS, 1% Triton X-100, 2 mM EDTA, 20 mM Tris-HCl [pH 8.1], and 500 mM NaCl), and buffer III (0.25 M LiCl, 1% NP-40, 1%

deoxycholate, 1 mM EDTA, and 10 mM Tris-HCl [pH 8.1]). Precipitates were then washed twice with TE buffer. Chromatin was eluted twice with 1% SDS, 0.1 M $NaHCO_3$ for 15 min and then decrosslinked in 225 μM NaCl for 12 hr at 65°C. The DNA was sequentially treated with RNase (50 μg/ml) at 37°C for 30 min and then proteinase K (100 μg/ml) at 37°C for 30 min, and then purified over a QIAquick spin column (QIAGEN) per the manufacturer's instructions. For quantitative PCR, 1 μl from a 40 μl DNA extraction was subjected to 40–50 cycles of PCR amplification. The result was analyzed as percent input after immunoprecipitation relative to the untreated control. The following PCR primers were used: *ERG* ChIP IV f: 5′-GAG GGA GAG GTG CAA ATT AGA G-3′ and *ERG* ChIP IV r: 5′-GGC TGA AGG ACA GGG ATT G-3′.

SUPPLEMENTAL INFORMATION

Supplemental Information includes four figures and can be found with this article online at http://dx.doi.org/10.1016/j.celrep.2013.06.039.

ACKNOWLEDGMENTS

This work was supported in part by CCSG P30 CA013696-36 via the Microscopy & Radiation Shared Resources and by NIH grants CA154293 (E.P.G.) and CA132813 (T.T.P.).

Received: December 30, 2012
Revised: May 29, 2013
Accepted: June 25, 2013
Published: July 25, 2013

REFERENCES

Asatiani, E., Huang, W.X., Wang, A., Rodriguez Ortner, E., Cavalli, L.R., Haddad, B.R., and Gelmann, E.P. (2005). Deletion, methylation, and expression of the NKX3.1 suppressor gene in primary human prostate cancer. Cancer Res. *65*, 1164–1173.

Bakkenist, C.J., and Kastan, M.B. (2003). DNA damage activates ATM through intermolecular autophosphorylation and dimer dissociation. Nature *421*, 499–506.

Bartek, J., and Lukas, J. (2003). Chk1 and Chk2 kinases in checkpoint control and cancer. Cancer Cell *3*, 421–429.

Bekker-Jensen, S., Lukas, C., Kitagawa, R., Melander, F., Kastan, M.B., Bartek, J., and Lukas, J. (2006). Spatial organization of the mammalian genome surveillance machinery in response to DNA strand breaks. J. Cell Biol. *173*, 195–206.

Bethel, C.R., Faith, D., Li, X., Guan, B., Hicks, J.L., Lan, F., Jenkins, R.B., Bieberich, C.J., and De Marzo, A.M. (2006). Decreased NKX3.1 protein expression in focal prostatic atrophy, prostatic intraepithelial neoplasia, and adenocarcinoma: association with gleason score and chromosome 8p deletion. Cancer Res. *66*, 10683–10690.

Bhaskara, V., Dupré, A., Lengsfeld, B., Hopkins, B.B., Chan, A., Lee, J.H., Zhang, X., Gautier, J., Zakian, V., and Paull, T.T. (2007). Rad50 adenylate kinase activity regulates DNA tethering by Mre11/Rad50 complexes. Mol. Cell *25*, 647–661.

Bowen, C., and Gelmann, E.P. (2010). NKX3.1 activates cellular response to DNA damage. Cancer Res. *70*, 3089–3097.

Bowen, C., Bubendorf, L., Voeller, H.J., Slack, R., Willi, N., Sauter, G., Gasser, T.C., Koivisto, P., Lack, E.E., Kononen, J., et al. (2000). Loss of NKX3.1 expression in human prostate cancers correlates with tumor progression. Cancer Res. *60*, 6111–6115.

Bowen, C., Stuart, A., Ju, J.H., Tuan, J., Blonder, J., Conrads, T.P., Veenstra, T.D., and Gelmann, E.P. (2007). NKX3.1 homeodomain protein binds to topoisomerase I and enhances its activity. Cancer Res. *67*, 455–464.

Chou, W.C., Wang, H.C., Wong, F.H., Ding, S.L., Wu, P.E., Shieh, S.Y., and Shen, C.Y. (2008). Chk2-dependent phosphorylation of XRCC1 in the DNA damage response promotes base excision repair. EMBO J. *27*, 3140–3150.

Ciccia, A., and Elledge, S.J. (2010). The DNA damage response: making it safe to play with knives. Mol. Cell *40*, 179–204.

Daniel, J.A., Pellegrini, M., Lee, J.H., Paull, T.T., Feigenbaum, L., and Nussenzweig, A. (2008). Multiple autophosphorylation sites are dispensable for murine ATM activation in vivo. J. Cell Biol. *183*, 777–783.

Ditch, S., and Paull, T.T. (2011). The ATM protein kinase and cellular redox signaling: beyond the DNA damage response. Trends Biochem. Sci. *37*, 15–22.

Fernandez-Capetillo, O., Lee, A., Nussenzweig, M., and Nussenzweig, A. (2004). H2AX: the histone guardian of the genome. DNA Repair (Amst.) *3*, 959–967.

Gelmann, E.P., Steadman, D.J., Ma, J., Ahronovitz, N., Voeller, H.J., Swope, S., Abbaszadegan, M., Brown, K.M., Strand, K., Hayes, R.B., and Stampfer, M.J. (2002). Occurrence of NKX3.1 C154T polymorphism in men with and without prostate cancer and studies of its effect on protein function. Cancer Res. *62*, 2654–2659.

Germann, M., Wetterwald, A., Guzmán-Ramirez, N., van der Pluijm, G., Culig, Z., Cecchini, M.G., Williams, E.D., and Thalmann, G.N. (2012). Stem-like cells with luminal progenitor phenotype survive castration in human prostate cancer. Stem Cells *30*, 1076–1086.

Grollman, A.P., and Moriya, M. (1993). Mutagenesis by 8-oxoguanine: an enemy within. Trends Genet. *9*, 246–249.

Guo, Z., Deshpande, R., and Paull, T.T. (2010a). ATM activation in the presence of oxidative stress. Cell Cycle *9*, 4805–4811.

Guo, Z., Kozlov, S., Lavin, M.F., Person, M.D., and Paull, T.T. (2010b). ATM activation by oxidative stress. Science *330*, 517–521.

He, H.H., Meyer, C.A., Shin, H., Bailey, S.T., Wei, G., Wang, Q., Zhang, Y., Xu, K., Ni, M., Lupien, M., et al. (2010). Nucleosome dynamics define transcriptional enhancers. Nat. Genet. *42*, 343–347.

Huang, X., King, M.A., Halicka, H.D., Traganos, F., Okafuji, M., and Darzynkiewicz, Z. (2004). Histone H2AX phosphorylation induced by selective photolysis of BrdU-labeled DNA with UV light: relation to cell cycle phase. Cytometry A *62*, 1–7.

Jackson, S.P., and Bartek, J. (2009). The DNA-damage response in human biology and disease. Nature *461*, 1071–1078.

Khalil, A., Morgan, R.N., Adams, B.R., Golding, S.E., Dever, S.M., Rosenberg, E., Povirk, L.F., and Valerie, K. (2011). ATM-dependent ERK signaling via AKT in response to DNA double-strand breaks. Cell Cycle *10*, 481–491.

Khalili, M., Mutton, L.N., Gurel, B., Hicks, J.L., De Marzo, A.M., and Bieberich, C.J. (2010). Loss of Nkx3.1 expression in bacterial prostatitis: a potential link between inflammation and neoplasia. Am. J. Pathol. *176*, 2259–2268.

Khanna, K.K., Keating, K.E., Kozlov, S., Scott, S., Gatei, M., Hobson, K., Taya, Y., Gabrielli, B., Chan, D., Lees-Miller, S.P., and Lavin, M.F. (1998). ATM associates with and phosphorylates p53: mapping the region of interaction. Nat. Genet. *20*, 398–400.

Kurz, E.U., and Lees-Miller, S.P. (2004). DNA damage-induced activation of ATM and ATM-dependent signaling pathways. DNA Repair (Amst.) *3*, 889–900.

Lee, J.H., and Paull, T.T. (2004). Direct activation of the ATM protein kinase by the Mre11/Rad50/Nbs1 complex. Science *304*, 93–96.

Lee, J.H., and Paull, T.T. (2005). ATM activation by DNA double-strand breaks through the Mre11-Rad50-Nbs1 complex. Science *308*, 551–554.

Lee, J.H., and Paull, T.T. (2006). Purification and biochemical characterization of ataxia-telangiectasia mutated and Mre11/Rad50/Nbs1. Methods Enzymol. *408*, 529–539.

Li, X., Guan, B., Maghami, S., and Bieberich, C.J. (2006). NKX3.1 is regulated by protein kinase CK2 in prostate tumor cells. Mol. Cell. Biol. *26*, 3008–3017.

Limoli, C.L., and Ward, J.F. (1993). A new method for introducing double-strand breaks into cellular DNA. Radiat. Res. *134*, 160–169.

Lin, X., Tascilar, M., Lee, W.H., Vles, W.J., Lee, B.H., Veeraswamy, R., Asgari, K., Freije, D., van Rees, B., Gage, W.R., et al. (2001). GSTP1 CpG island

hypermethylation is responsible for the absence of GSTP1 expression in human prostate cancer cells. Am. J. Pathol. *159*, 1815–1826.

Lin, C., Yang, L., Tanasa, B., Hutt, K., Ju, B.G., Ohgi, K., Zhang, J., Rose, D.W., Fu, X.D., Glass, C.K., and Rosenfeld, M.G. (2009). Nuclear receptor-induced chromosomal proximity and DNA breaks underlie specific translocations in cancer. Cell *139*, 1069–1083.

Mani, R.S., Tomlins, S.A., Callahan, K., Ghosh, A., Nyati, M.K., Varambally, S., Palanisamy, N., and Chinnaiyan, A.M. (2009). Induced chromosomal proximity and gene fusions in prostate cancer. Science *326*, 1230.

Markowski, M.C., Bowen, C., and Gelmann, E.P. (2008). Inflammatory cytokines induce phosphorylation and ubiquitination of prostate suppressor protein NKX3.1. Cancer Res. *68*, 6896–6901.

Miao, Z.H., Player, A., Shankavaram, U., Wang, Y.H., Zimonjic, D.B., Lorenzi, P.L., Liao, Z.Y., Liu, H., Shimura, T., Zhang, H.L., et al. (2007). Nonclassic functions of human topoisomerase I: genome-wide and pharmacologic analyses. Cancer Res. *67*, 8752–8761.

Murata, M., Thanan, R., Ma, N., and Kawanishi, S. (2012). Role of nitrative and oxidative DNA damage in inflammation-related carcinogenesis. J. Biomed. Biotechnol. *2012*, 623019.

Nelson, W.G., De Marzo, A.M., and Isaacs, W.B. (2003). Prostate cancer. N. Engl. J. Med. *349*, 366–381.

Nupponen, N.N., Wallén, M.J., Ponciano, D., Robbins, C.M., Tammela, T.L., Vessella, R.L., Carpten, J.D., and Visakorpi, T. (2004). Mutational analysis of susceptibility genes RNASEL/HPC1, ELAC2/HPC2, and MSR1 in sporadic prostate cancer. Genes Chromosomes Cancer *39*, 119–125.

Ouyang, X., DeWeese, T.L., Nelson, W.G., and Abate-Shen, C. (2005). Loss-of-function of Nkx3.1 promotes increased oxidative damage in prostate carcinogenesis. Cancer Res. *65*, 6773–6779.

Parlanti, E., Fortini, P., Macpherson, P., Laval, J., and Dogliotti, E. (2002). Base excision repair of adenine/8-oxoguanine mispairs by an aphidicolin-sensitive DNA polymerase in human cell extracts. Oncogene *21*, 5204–5212.

Pascucci, B., Maga, G., Hübscher, U., Bjoras, M., Seeberg, E., Hickson, I.D., Villani, G., Giordano, C., Cellai, L., and Dogliotti, E. (2002). Reconstitution of the base excision repair pathway for 7,8-dihydro-8-oxoguanine with purified human proteins. Nucleic Acids Res. *30*, 2124–2130.

Paull, T.T., and Lee, J.H. (2005). The Mre11/Rad50/Nbs1 complex and its role as a DNA double-strand break sensor for ATM. Cell Cycle *4*, 737–740.

Pollack, A., and Zagars, G.K. (1997). External beam radiotherapy dose response of prostate cancer. Int. J. Radiat. Oncol. Biol. Phys. *39*, 1011–1018.

Pollack, A., Zagars, G.K., Smith, L.G., Lee, J.J., von Eschenbach, A.C., Antolak, J.A., Starkschall, G., and Rosen, I. (2000). Preliminary results of a randomized radiotherapy dose-escalation study comparing 70 Gy with 78 Gy for prostate cancer. J. Clin. Oncol. *18*, 3904–3911.

Rouet, P., Smih, F., and Jasin, M. (1994). Introduction of double-strand breaks into the genome of mouse cells by expression of a rare-cutting endonuclease. Mol. Cell. Biol. *14*, 8096–8106.

Seppälä, E.H., Ikonen, T., Autio, V., Rökman, A., Mononen, N., Matikainen, M.P., Tammela, T.L., and Schleutker, J. (2003). Germ-line alterations in MSR1 gene and prostate cancer risk. Clin. Cancer Res. *9*, 5252–5256.

Shen, M.M., and Abate-Shen, C. (2010). Molecular genetics of prostate cancer: new prospects for old challenges. Genes Dev. *24*, 1967–2000.

Tan, P.Y., Chang, C.W., Chng, K.R., Wansa, K.D., Sung, W.K., and Cheung, E. (2012). Integration of regulatory networks by NKX3-1 promotes androgen-dependent prostate cancer survival. Mol. Cell. Biol. *32*, 399–414.

Tomlins, S.A., Rhodes, D.R., Perner, S., Dhanasekaran, S.M., Mehra, R., Sun, X.W., Varambally, S., Cao, X., Tchinda, J., Kuefer, R., et al. (2005). Recurrent fusion of TMPRSS2 and ETS transcription factor genes in prostate cancer. Science *310*, 644–648.

Wang, L., McDonnell, S.K., Cunningham, J.M., Hebbring, S., Jacobsen, S.J., Cerhan, J.R., Slager, S.L., Blute, M.L., Schaid, D.J., and Thibodeau, S.N. (2003). No association of germline alteration of MSR1 with prostate cancer risk. Nat. Genet. *35*, 128–129.